

Low-Loss Characteristics of Metal-Foil-Based Passive Components by Surface-Activated Bonding Technologies

Keita Matsuura¹, Jianbo Liang, *Member, IEEE*, Koichi Maezawa, *Member, IEEE*,
and Naoteru Shigekawa¹, *Member, IEEE*

Abstract—Low-loss passive components for RF signals compatible with the on-wafer process are essential for realizing integrated circuits with high-frequency and high-power operations. We successfully fabricate thick-metal-film-based coplanar waveguides (CPWs) and inductors (INDs) by directly bonding a 17- μm -thick Al foil to a sapphire (0001) substrate and wet etching. The surface-activated bonding (SAB) technologies at room temperature are used. RF characteristics of the foil-based passive components are compared with those of components made of 1- μm -thick evaporated Al layers. We obtain a better insertion loss and a higher Q -factor for foil-based CPWs and INDs, respectively. The measured characteristics are compared with those obtained by an analysis based on the equivalent circuit scheme. Impacts of side etching of foils and surface oxidation on their characteristics are observed. Characteristics of virtual components made of 1- μm -thick Al foils, i.e., 1- μm -thick Al films with the same resistivity as that of foils, are analytically investigated.

Index Terms—Al foil, conductor loss, coplanar waveguide (CPW), high- Q , inductor (IND), surface-activated bonding (SAB).

I. INTRODUCTION

LOW-LOSS passive devices for RF signals are strongly required in microwave monolithic integrated circuits (MMICs) [1], sensors, actuators, and wireless modules since their performances are limited by the characteristics of the passive components. In addition, systems for wireless communications such as cellular phones, wireless LANs, and bluetooth require high- Q inductors (INDs) in the matching circuits of the antennae, surface acoustic wave filters [2], and power amplifiers (PAs) [3]. Given that the loss of components at several 10 GHz is determined by the dielectric properties of

substrates (dielectric loss) and the resistance of metal layers (ohmic loss), the usage of thicker metal films is strongly required in RF interconnects such as coplanar waveguides (CPWs) [4]–[10] and CPW INDs [11]. Thicknesses of metal films for integrated on-chip passive components have been limited up to a few microns [4], [12], [13], which is assumed to cause the ohmic loss and limit their performances.

Thick-metal films are conventionally fabricated by means of high-speed deposition, sputtering, or electroplating. Note, however, that the thickness of metal films in the above methods determines the period of processing, and hence the cost. In [11], meander-type CPW INDs were reportedly fabricated on a flexible plastic polyimide foil using the ink-jet printing technology with silver nanoparticle ink in a single layer. The advantages of ink-jet printing technology are waste reduction, no mask requirements, and reduction in processing steps. The thickness of nanoparticle layers fabricated in that work was, however, limited to 1 μm .

The bonding of metal foils using adhesives or resin, which are generally employed in fabricating transmission lines for RF signals on circuit boards, must be avoided in the on-wafer process for fabricating MMICs or PAs. We previously applied the surface-activated bonding (SAB) technologies [14]–[17] for fabricating junctions made of dissimilar semiconductor materials without intermediate materials. In the SAB process, the surfaces of dissimilar materials are activated by using the fast atom beams of Ar in ultrahigh vacuum so that the native oxide layers formed on surfaces of samples are removed. We reported on the performances of advanced devices such as III–V-on-Si multijunction solar cells [17] composed of the SAB-based heterojunctions. We also bonded a several-10- μm -thick Al foil to Si and SiC substrates and examined the possibility of Al foils for ultrathick ohmic or Schottky contacts [18], [19]. Regardless of the thickness of Al foils, the SAB process can be completed in a short period.

We assume that because of the excellent dielectric characteristics, sapphire substrates are ideal as a testbed for examining the contribution of ohmic loss of passive components. It is also notable that sapphire substrates have been widely utilized for the epitaxial growth of GaN HEMT PAs. Recently, we provided a brief report on CPWs fabricated on Al foils directly bonded to a sapphire (0001) substrate [20].

Manuscript received March 17, 2019; revised May 26, 2019; accepted July 10, 2019. This work was supported in part by the Japan Science and Technology Agency through the Matching Planner Programs. The review of this paper was arranged by Editor G. Niu. (*Corresponding author: Naoteru Shigekawa.*)

K. Matsuura, J. Liang, and N. Shigekawa are with the Graduate School of Engineering, Osaka City University, Osaka 558-8585, Japan (e-mail: shigekawa@eng.osaka-cu.ac.jp).

K. Maezawa is with the Department of Electric and Electronic Engineering, University of Toyama, Toyama 930-0887, Japan.

Color versions of one or more of the figures in this paper are available online at <http://ieeexplore.ieee.org>.

Digital Object Identifier 10.1109/TED.2019.2928620

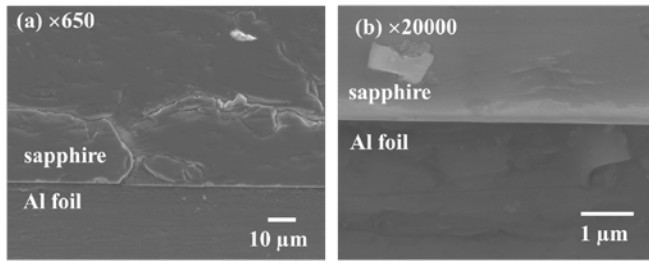


Fig. 1. Field-emission scanning electron microscope image of a bonding interface of an Al-foil/sapphire junction with a magnification scale of (a) 650 \times and (b) 20 000 \times .

In this paper, we describe the process for bonding Al foils to sapphire substrates and fabricating passive components. Then, we discuss the RF characteristics of fabricated meander-type INDs as well as CPWs. The thickness of the used foils is 17 μm . The characteristics of passive components made of evaporated 1- μm -thick Al layers are examined for comparison. These characteristics are discussed in conjunction with the RF resistance of metal films. An equivalent circuit of INDs is introduced for discussing their characteristics. The characteristics of virtual 1- μm -thick foil-based components, i.e., devices made of films with the same resistivity as that of 17- μm Al foils, are also examined.

II. FABRICATION OF COPLANAR WAVEGUIDES AND INDUCTORS

Using the SAB, we bonded an Al foil with a thickness $t = 17 \mu\text{m}$ to a 420- μm -thick sapphire (0001) substrate without heating. The SAB condition employed in the work was previously reported [15]. The roughness average of the substrate surface was 0.2–0.3 nm, which was small enough for the success of direct bonding. The bonding strength was sufficiently large so that there was no delamination at the interfaces even after the etching and dicing processes. The Al foil/sapphire interface was examined by using a field-emission scanning electron microscope. Obtained images with different magnifications are shown in Fig. 1(a) and (b). As observed from the figures, we found that Al foil and sapphire were firmly bonded without gaps.

A 7-mm-long single-line wire was prepared by etching the foil using a mixture of H_3PO_4 , HNO_3 , CH_3COOH , and H_2O ($\text{H}_3\text{PO}_4:\text{HNO}_3:\text{CH}_3\text{COOH}:\text{H}_2\text{O} = 16:1:2:1$). The etching rate of Al films was $\sim 4 \mu\text{m/h}$. By measuring the current–voltage characteristics of the wire, the sheet resistance R_{sh} and resistivity ρ of the Al foil were found to be 1.6 $\text{m}\Omega/\text{sq.}$ and 2.7 $\mu\Omega\cdot\text{cm}$, respectively. We also evaporated a 1- μm -thick Al layer on a sapphire substrate and found that R_{sh} and ρ of the evaporated Al layer were 36 $\text{m}\Omega/\text{sq.}$ and 3.6 $\mu\Omega\cdot\text{cm}$, respectively. R_{sh} and ρ of each Al film are shown in Table I.

We designed CPWs with lengths l of 1.5, 3, 4.5, 6, and 8 mm. The 8-mm-long CPW was meander-shaped while CPWs with other lengths were straight. The signal-linewidth W and slot width S were determined so that the characteristic impedance of 50 Ω was achieved [10]. The nominal W and S of Al-foil CPWs (CPW-A) were preset to be 100 and 50 μm , respectively. The nominal W and S of CPWs of 1- μm -Al

TABLE I
GEOMETRICAL AND MATERIAL PROPERTIES OF CPW-A AND CPW-B

| | CPW-A (Al foil) | CPW-B (evaporation) |
|---------------------------|--|--------------------------------|
| Signal-line width (W) | 100 μm | 110 μm |
| Slot width (S) | 50 μm | 40 μm |
| Metal thickness (t) | 17 μm | 1 μm |
| Sheet resistance | 1.6 $\text{m}\Omega/\text{sq.}$ | 36 $\text{m}\Omega/\text{sq.}$ |
| Resistivity (ρ) | 2.7 $\mu\Omega\cdot\text{cm}$ | 3.6 $\mu\Omega\cdot\text{cm}$ |
| Length/shape | 1.5, 3, 4.5, 6 mm (straight) 8 mm (meander) | |

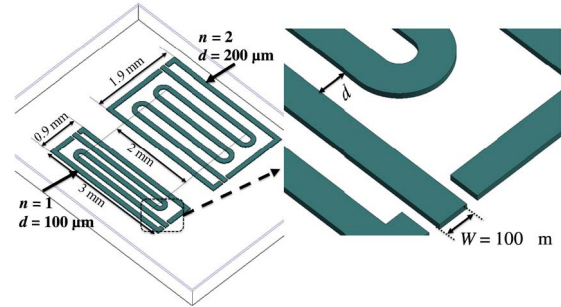


Fig. 2. Geometries of INDs with $n = 1$, $d = 100 \mu\text{m}$ and $n = 2$, $d = 200 \mu\text{m}$.

layers (CPW-B) were 110 and 40 μm , respectively. The effects of the side etching were ignored for the 1- μm -thick film. The difference in the optimum W and S between CPW-A and CPW-B is due to the thicknesses of Al films of the respective CPWs. The geometries of CPWs are also summarized in Table I.

The INDs were made of two-port ground-signal-ground structure with meander-shaped signal lines. The number of turns in the meanders n was 1, 2, or 3. The spacing between adjacent segments in the meanders d was 100, 200, or 300 μm . We completely fabricated nine types of INDs with different combinations of n and d . W of all INDs was fixed to 100 μm . The same design was applied for INDs made of Al foils (IND-A) and INDs made of evaporated Al layers (IND-B). Fig. 2 shows the geometry of INDs with $n = 1$, $d = 100 \mu\text{m}$ and $n = 2$, $d = 200 \mu\text{m}$.

A top view of 8-mm-long meander-shaped CPW-A is shown in Fig. 3(a). W and S of the CPW-A were found to be 90 ± 20 and $60 \pm 20 \mu\text{m}$, respectively. A top view of an IND-A with $n = 3$ and $d = 200 \mu\text{m}$ is partly shown in Fig. 3(b). Its W and d were 90 ± 20 and $210 \pm 20 \mu\text{m}$, respectively. Such large fluctuations of these structural parameters of CPWs and INDs were likely to be attributed to the erosion of sides of Al foils during the wet etching. We actually confirmed (not depicted) that the cross section of signal lines of Al foils was of trapezoidal-shaped due to the side etching.

We measured S-parameters of CPWs and INDs at frequencies between 40 MHz and 20 GHz using a vector network analyzer.

III. MODEL OF INDUCTORS

Fig. 4(a) shows a π -shaped equivalent circuit of two-port INDs [21]. The contributions of Y-parameters of INDs are also shown. In this figure, R_s and L_s are a resistance and

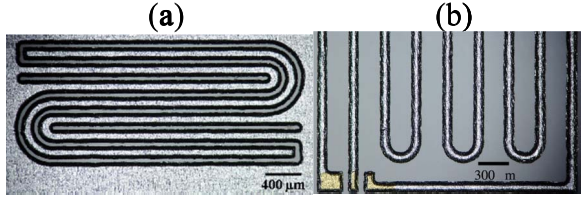


Fig. 3. Top view of (a) 8-mm-long meander-shaped CPW-A and (b) IND-A with $n = 3$ and $d = 200 \mu\text{m}$. (a) Its W and S were 90 ± 20 and $60 \pm 20 \mu\text{m}$ and (b) W and d were 90 ± 20 and $210 \pm 20 \mu\text{m}$, respectively.

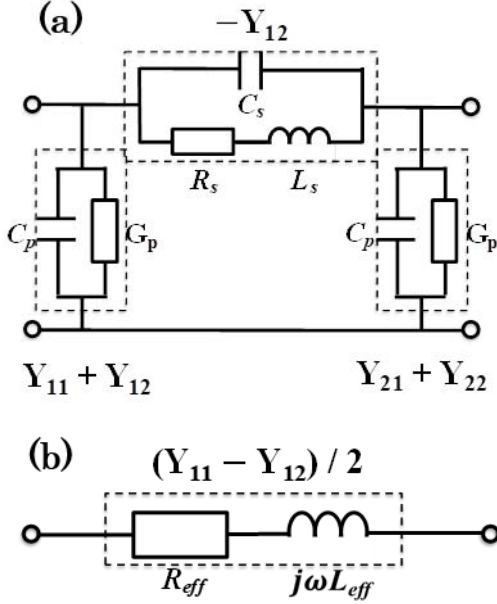


Fig. 4. (a) π -type equivalent circuit of two-port INDs. (b) Model of the conductance along the signal lines of INDs.

an inductance of the meander-shaped signal lines. C_s is a capacitance indicating the electrical coupling between their segments. C_p and G_p are a capacitance and a conductance between signal lines and ground planes, respectively.

By considering the skin effects, R_s is approximately given by the following R_{model} :

$$R_s \approx R_{\text{model}} = \begin{cases} \rho l / (Wt) & (\text{for } \delta > t/2) \\ \rho l / \{2\delta(W + t) - 4\delta^2\} & (\text{for } \delta < t/2) \end{cases} \quad (1)$$

where δ denotes the skin depth ($\delta = (\rho / \pi f \mu_0)^{1/2}$). This expression is based on a simple scheme that in the case of $\delta < t/2$ the conductive parts with the thickness of δ formed on the surface, backside, and two sides of Al films independently contribute to the electrical conduction. We find that at 40 MHz, or the lowest frequency in measurements of RF characteristics in this paper, $\delta > t/2$ holds both in the Al foil and evaporated Al layer.

We assume that L_s is equal to an analytically calculated value L_{model} [22], [23], which is obtained by summing self-inductances of respective straight segments in a signal line and mutual inductances of neighboring antiparallel segments.

The conductance between the two signal ports shown in Fig. 4(a) is modeled as the serial-connected effective inductance L_{eff} and effective resistance R_{eff} as is shown in

Fig. 4(b). We assume that the dc conductivity between the signal lines and the ground planes of INDs is negligible ($G_p = 0$). On this assumption, we analytically express R_{eff} and L_{eff} , which are denoted as $R_{\text{eff,calc}}$ and $L_{\text{eff,calc}}$, as

$$\begin{aligned} R_{\text{eff,calc}} &= \frac{R_s}{\{1 - \omega^2 L_s (C_p/2 + C_s)\}^2 + \{\omega (C_p/2 + C_s) R_s\}^2} \\ &\approx \frac{R_{\text{model}}}{\{1 - \omega^2 L_{\text{model}} (C_p/2 + C_s)\}^2 + \{\omega (C_p/2 + C_s) R_{\text{model}}\}^2} \end{aligned} \quad (2)$$

and

$$\begin{aligned} L_{\text{eff,calc}} &= \frac{L_s \{1 - \omega^2 L_s (C_p/2 + C_s)\} - (C_p/2 + C_s) R_s^2}{\{1 - \omega^2 L_s (C_p/2 + C_s)\}^2 + \{\omega (C_p/2 + C_s) R_s\}^2} \\ &\approx \frac{L_{\text{model}} \{1 - \omega^2 L_{\text{model}} (C_p/2 + C_s)\} - (C_p/2 + C_s) R_{\text{model}}^2}{\{1 - \omega^2 L_{\text{model}} (C_p/2 + C_s)\}^2 + \{\omega (C_p/2 + C_s) R_{\text{model}}\}^2} \end{aligned} \quad (3)$$

respectively.

Using (3) and assuming that $L_s \gg (C_p/2 + C_s) R_s^2$, the self-resonance frequency (SRF), or the frequency corresponding to $L_{\text{eff}} = 0$, is expressed as

$$\begin{aligned} \text{SRF} &= \frac{1}{2\pi} \sqrt{\frac{1}{L_s (C_p/2 + C_s)} - \left(\frac{R_s}{L_s}\right)^2} \\ &\approx \frac{1}{2\pi \sqrt{L_{\text{model}} (C_p/2 + C_s)}}. \end{aligned} \quad (4)$$

Then, we obtain

$$C_p/2 + C_s \approx \frac{1}{(2\pi \cdot \text{SRF})^2 L_{\text{model}}}. \quad (5)$$

Because of the symmetric properties of INDs, Y_{21} and Y_{22} should be equal to Y_{12} and Y_{11} , respectively. The conductance along the signal line is, then, given by $(Y_{11} - Y_{12})/2$. Consequently, measurement-based L_{eff} , R_{eff} , and Q -factor of INDs ($L_{\text{eff,meas}}$, $R_{\text{eff,meas}}$, and Q_{meas}) are expressed as

$$L_{\text{eff,meas}} = \frac{\text{Im}\left(\frac{2}{Y_{11} - Y_{12}}\right)}{2\pi f} \quad (6)$$

$$R_{\text{eff,meas}} = \text{Re}\left(\frac{2}{Y_{11} - Y_{12}}\right) \quad (7)$$

and

$$Q_{\text{meas}} \equiv \frac{2\pi f L_{\text{eff,meas}}}{R_{\text{eff,meas}}} = -\frac{\text{Im}(Y_{11} - Y_{12})}{\text{Re}(Y_{11} - Y_{12})} \quad (8)$$

respectively [11]. These equations are used for experimentally extracting L_{eff} , R_{eff} , Q -factor, and SRF.

IV. RESULTS

A. RF Characteristics of CPWs

Fig. 5(a) and (b) compare the transmission characteristics ($|S_{21}|$) of 3- and 8-mm-long CPWs, respectively. In the case of 3-mm-long CPWs, $|S_{21}|$ of CPW-A was larger than -1.0 dB over the almost entire frequency range, while $|S_{21}|$ of CPW-A

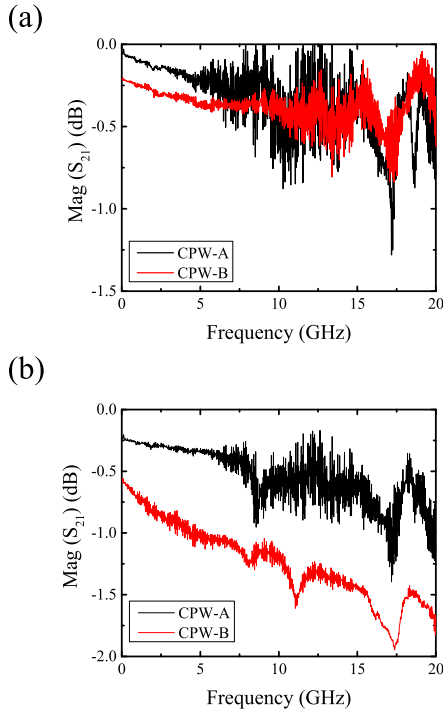


Fig. 5. Transmission characteristics for (a) 3-mm CPWs and (b) 8-mm CPWs, respectively.

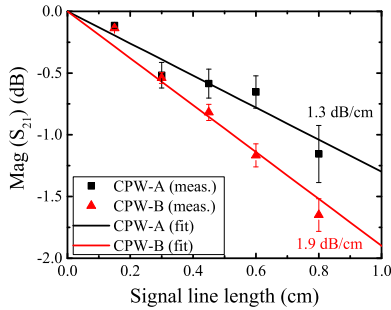


Fig. 6. Relationships between the insertion loss and the length for the two types of CPWs at 20 GHz.

was slightly larger than that of CPW-B over the almost entire frequency range, as is shown in Fig. 5(a). In the case of 8-mm-long CPWs, $|S_{21}|$ of CPW-A was larger than -1.2 dB at 20 GHz. $|S_{21}|$ of CPW-B was, however, as small as -1.8 dB at 20 GHz. We also observed a discrepancy of $|S_{21}|$ from 0 dB at the dc limit.

Relationships between measured $|S_{21}|$ at 20 GHz and signal line length are shown in Fig. 6. At this frequency, the measured insertion loss per unit length (attenuation constant α) was 1.3 and 1.9 dB/cm for CPW-A and CPW-B, respectively. It is notable that the insertion loss for CPW-A was smaller than the loss of CPWs made of 4- μm -thick electroplated Au films on a semi-insulating substrate (~ 1.7 dB/cm) at 20 GHz [4].

At 20 GHz, δ was 0.59 and 0.67 μm for the Al foil and evaporated Al layer, respectively. Then, surface resistance [24] at this frequency was estimated to be 46 and 72 $\text{m}\Omega/\text{sq}$. for 17- μm -thick Al foils and 1- μm -thick evaporated Al layers. A larger surface resistance might be obtained for the 1- μm -thick films based on a more precise analysis [24]. Using these

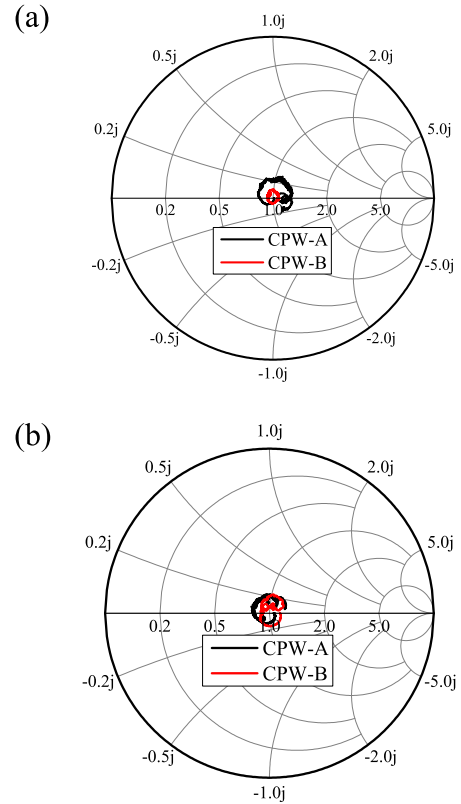


Fig. 7. Return loss characteristics for (a) 3-mm CPWs and (b) 8-mm CPWs, respectively.

resistance values in combination with [10], the loss due to the resistance of the conductors, or the conductor loss α_c , was estimated to be 0.41 and 1.07 dB/cm at 20 GHz for the CPW-A and CPW-B, respectively.

Fig. 7(a) and (b) show the return loss of 3- and 8-mm-long CPWs, respectively. As is seen from the two figures, the trajectory of S_{11} of the CPW-A more largely deviated from the center in comparison with the CPW-B, which suggested that the impedance mismatching was more marked in the CPW-A.

B. RF Characteristics of INDs

The measured S-parameters of the respective INDs were converted to Y-parameters. Using (6)–(8), we extracted $L_{\text{eff, meas}}$, $R_{\text{eff, meas}}$, and Q_{meas} . Fig. 8(a)–(c) show these values of an IND-A and IND-B with $n = 3$ and $d = 300$ μm as typical results. The SRF, which defined the range of frequencies where the equivalent circuit shown in Fig. 2(a) and (b) was valid, was 3.87 and 3.57 GHz for the IND-A and IND-B, respectively.

As seen from Fig. 8(a), $L_{\text{eff, meas}}$ of IND-A almost agreed with that of IND-B. In contrast, as shown in Fig. 8(b), $R_{\text{eff, meas}}$ of IND-A was smaller than that of IND-B. At 40 MHz, or the low-frequency limit, $R_{\text{eff, meas}}$ of IND-A was approximately 1/10 of $R_{\text{eff, meas}}$ of IND-B. As the frequency increased, $R_{\text{eff, meas}}$ of both INDs increased so that the difference in $R_{\text{eff, meas}}$ became negligibly small. Due to the smaller $R_{\text{eff, meas}}$, the IND-A outperformed the IND-B in terms of the Q -factor.

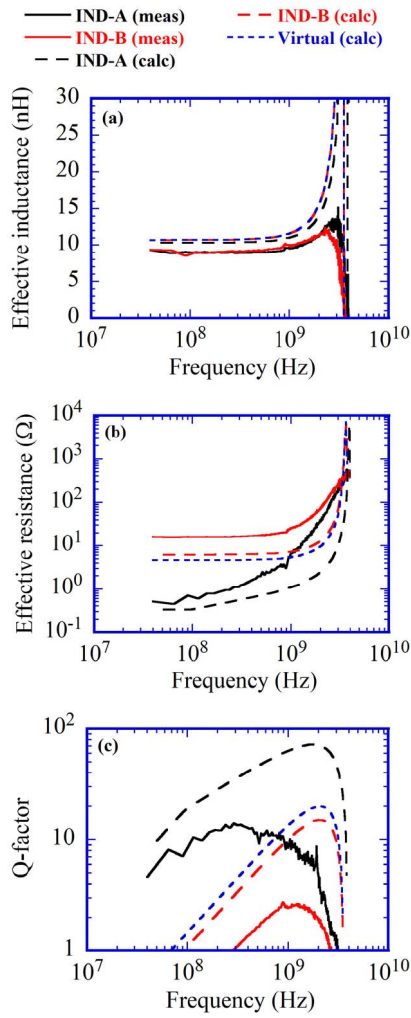


Fig. 8. Measured and calculated (a) effective inductances, (b) effective resistances, and (c) Q -factors for INDs with $n = 3$ and $d = 300 \mu\text{m}$.

The maximum of Q -factor, Q_{max} , of the IND-A was 14, which was six times larger than Q_{max} of the IND-B as shown in Fig. 8(c). Q_{max} of the IND-A was ~ 4 times larger than Q_{max} of coplanar-type INDs made of Ag nanoparticle layers reported in [11], which was due to the difference in conductor thicknesses.

Using (5), we estimated $C_p/2 + C_s$ to be 0.16 and 0.19 pF for the IND-A and IND-B, respectively. $L_{\text{eff,calc}}$, $R_{\text{eff,calc}}$, and Q -factor, Q_{calc} , were obtained by using the above capacitance values. They are compared with measurements in the respective figures.

Fig. 8(a) shows that similar to measurements, $L_{\text{eff,calc}}$ of IND-A almost agreed with that of IND-B in the entire frequency range. $L_{\text{eff,calc}}$ was not sensitive to the frequency up to 1 GHz. For $f > 1$ GHz, it rose abruptly because the denominator in (3) decreased. The increase of $L_{\text{eff,calc}}$ was more rapid than measurement.

Given that we had $\delta < t/2$ in the 17- μm -thick Al foil at frequencies higher than 100 MHz, R_{model} was scaled as $R_{\text{model}} \propto \delta^{-1} \propto f^{1/2}$ for $f > 100$ MHz in the IND-A. $R_{\text{eff,calc}}$ of the IND-A revealed a similar dependence on the frequency up to ~ 1 GHz as shown in Fig. 8(b). $R_{\text{eff,calc}}$ of IND-A

abruptly rose for $f > 1$ GHz. In the 1- μm -thick evaporated Al layer, in contrast, we had $\delta > t/2$ at frequencies up to 10 GHz. R_{model} and, hence, $R_{\text{eff,calc}}$ of the IND-B were, consequently, independent of the frequency up to ~ 1 GHz. Similar to $R_{\text{eff,calc}}$ of IND-A, $R_{\text{eff,calc}}$ of IND-B abruptly rose for $f > 1$ GHz. $R_{\text{eff,calc}}$ was 1/10 (IND-A) \sim 1/3 (IND-B) of measured $R_{\text{eff,meas}}$ in the entire frequency range, which explained a large difference in Q -factors between measurement and calculation as shown in Fig. 8(c). A better agreement might be obtained by optimizing the resistivity of conductors and employing a more precise approach such as the electromagnetic field analysis.

Table II summarizes $L_{\text{eff,meas}}$ at 40 MHz, $L_{\text{eff,calc}}$ at 40 MHz, $R_{\text{eff,meas}}$ at 40 MHz, $R_{\text{eff,calc}}$ at 40 MHz, Q_{max} , the frequency for Q_{max} , or $F_{Q_{\text{max}}}$, and the SRF of the respective INDs. $L_{\text{eff,meas}}$ at 40 MHz is compared with $L_{\text{eff,calc}}$ at 40 MHz of the respective INDs shown in Fig. 9(a). $R_{\text{eff,meas}}$ at 40 MHz is compared with $R_{\text{eff,calc}}$ at 40 MHz as shown in Fig. 9(b). Straight lines for $L_{\text{eff,meas}} = L_{\text{eff,calc}}$ and $R_{\text{eff,meas}} = R_{\text{eff,calc}}$ are shown in the respective figures as a guide of eyes. $L_{\text{eff,meas}}$ was 8%–50% smaller than $L_{\text{eff,calc}}$. $R_{\text{eff,meas}}$ of the IND-As was largely scattered and was ~ 10 times higher than $R_{\text{eff,calc}}$ at maximum. $R_{\text{eff,meas}}$ of the IND-Bs was 2–3 times higher than their $R_{\text{eff,calc}}$.

V. DISCUSSION

It is noteworthy that the difference in α_c between CPW-A and CPW-B (0.66 dB/cm) was close to the difference in the measured α between the two CPWs (0.6 dB/cm), which means that the lower α of CPW-A is attributable to its thicker conductor with lower resistivity. Higher Q -factors of IND-A than Q -factors of IND-B are similarly explained. These results together with better performances of CPW-A and IND-A in comparison with [4] or [11] show the superiority of the proposed method, i.e., direct bonding of thick foils, for realizing passive components with high performances.

The surface resistance of virtual 1- μm -thick Al foils was 54 m Ω/\square at 20 GHz. Then, α_c of the virtual CPW at this frequency was estimated to be 0.80 dB/cm, lower than that of the CPW-B by 0.27 dB/cm. $R_{\text{eff,calc}}$ and Q_{calc} for the virtual IND are shown in Fig. 8(b) and (c), respectively. $R_{\text{eff,calc}}$ of the virtual IND was 25% smaller in comparison with $R_{\text{eff,calc}}$ of the IND-B, which brought about a larger Q_{calc} for the virtual IND. Higher Q -factor of the virtual IND as well as lower α_c of the virtual CPW suggests that the direct bonding of metal foils is assumed to be helpful even in the case that the thickness of bonded foils is similar to that of evaporated metal layers.

The difference between $R_{\text{eff,meas}}$ and $R_{\text{eff,calc}}$ at 40 MHz might be attributed to the oxidation of Al films. The result that $R_{\text{eff,meas}}$ of the IND-As is markedly scattered in comparison with the IND-Bs is attributed to the erosion in the Al foils. The deviation of S_{11} from the origin observed in the RF characteristics of the CPW-A [Fig. 7(a) and (b)] is explained in the same scheme. Passive components with more excellent performances could be realized by employing the dry etching process of bonded metal foils and controlling their surface oxidation.

TABLE II
EXTRACTED VALUES OF PARAMETERS DEFINING RF CHARACTERISTICS OF (A) IND-As and (B) IND-Bs

| d (μm) | 100 | | | 200 | | | 300 | | |
|---|------|------|------|------|------|------|------|------|------|
| n | 1 | 2 | 3 | 1 | 2 | 3 | 1 | 2 | 3 |
| Signal-line length (mm) | 7.63 | 12.3 | 16.9 | 7.94 | 12.9 | 17.8 | 8.26 | 13.5 | 18.8 |
| $L_{\text{eff, meas}}$ at 40 MHz (nH) | 2.6 | 4.8 | 6.9 | 3.9 | 6.3 | 7.9 | 4.2 | 7.0 | 9.6 |
| $L_{\text{eff, calc}}$ at 40 MHz (nH) | 4.4 | 6.3 | 8.2 | 4.8 | 7.1 | 9.2 | 5.2 | 7.8 | 11 |
| $R_{\text{eff, meas}}$ at 40 MHz (Ω) | 2.3 | 1.2 | 1.0 | 1.1 | 3.6 | 4.5 | 1.1 | 1.4 | 0.5 |
| $R_{\text{eff, calc}}$ at 40 MHz (Ω) | 0.12 | 0.20 | 0.27 | 0.13 | 0.20 | 0.28 | 0.13 | 0.21 | 0.30 |
| Q_{max} | 5.4 | 7.5 | 8.3 | 5.6 | 6.2 | 9.6 | 9.2 | 9.5 | 14.3 |
| $F_{Q_{\text{max}}}$ (GHz) | 1.6 | 0.8 | 0.6 | 1.3 | 1.1 | 0.6 | 0.8 | 0.8 | 0.3 |
| SRF (GHz) | 10.4 | 6.6 | 4.6 | 9.5 | 5.0 | 4.4 | 8.4 | 4.8 | 3.9 |

| (B) | | | | | | | | | |
|---|------|------|------|-----|------|------|-----|------|------|
| d (μm) | 100 | | | 200 | | | 300 | | |
| n | 1 | 2 | 3 | 1 | 2 | 3 | 1 | 2 | 3 |
| $L_{\text{eff, meas}}$ at 40 MHz (nH) | 2.9 | 4.3 | 5.9 | 3.8 | 6.1 | 8.4 | 4.4 | 7.0 | 9.9 |
| $L_{\text{eff, calc}}$ at 40 MHz (nH) | 4.3 | 6.2 | 8.0 | 4.8 | 7.0 | 9.3 | 5.1 | 7.7 | 10 |
| $R_{\text{eff, meas}}$ at 40 MHz (Ω) | 7.7 | 11.0 | 13.9 | 7.8 | 12.1 | 15.5 | 9.1 | 13.2 | 16.4 |
| $R_{\text{eff, calc}}$ at 40 MHz (Ω) | 2.7 | 4.4 | 6.1 | 2.9 | 4.6 | 6.4 | 3.0 | 4.9 | 6.8 |
| Q_{max} | 2.9 | 2.5 | 2.3 | 3.1 | 2.8 | 2.5 | 3.0 | 2.8 | 2.6 |
| $F_{Q_{\text{max}}}$ (GHz) | 2.0 | 1.9 | 1.8 | 1.8 | 1.6 | 1.3 | 1.8 | 1.4 | 1.2 |
| SRF (GHz) | 10.0 | 6.1 | 4.8 | 9.4 | 5.0 | 3.9 | 8.4 | 4.6 | 3.6 |

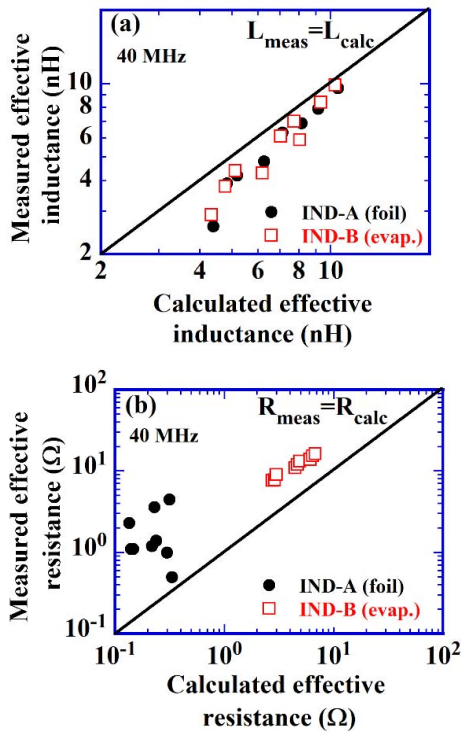


Fig. 9. Relationships between (a) measured and calculated L_{eff} at 40 MHz and (b) measured and calculated R_{eff} at 40 MHz. Guides for eyes are also shown.

We observed a 0.8–0.9 dB/cm discrepancy between the measured α and calculated α_c for the CPW-A and CPW-B. The discrepancy might be due to the substrate loss, radiation loss, and the uncertainty in the estimated surface resistance. Using a reported loss tangent of sapphire ($\tan\delta \sim 1\text{E-}5$ for 21.4–21.7 GHz at room temperature) [25], the substrate loss of each CPW at 20 GHz was assumed to be negligibly small (< 0.01 dB/cm), which suggested that other two factors should be dominant.

VI. CONCLUSION

We directly bonded a 17- μm -thick Al foil to a sapphire substrate by using the SAB technology. We fabricated CPWs and two-port INDs by patterning the bonded Al foils by wet etching. The RF characteristics of the Al-foil CPWs (CPW-A) and INDs (IND-A) were better than the characteristics of the CPWs and INDs fabricated on a 1- μm -thick evaporated Al layer (CPW-B and IND-B) because of the lower resistance of foils. An analysis predicted that virtual components made of 1- μm -thick Al foils outperformed the CPW-B and IND-B in the RF characteristics. These results suggested that the direct bonding of metal foils was promising for fabricating passive components with excellent RF characteristics. The characteristics of the fabricated components were in qualitative agreement with results of calculation using an equivalent circuit model. Parasitic effects on the characteristics of the CPW-A and IND-A due to the erosion of sides of signal lines and the oxidation of their surfaces were observed. The characteristics of foil-based passive components were assumed to be improved by more precisely controlling the shape of cross section of the signal lines and suppressing the oxidation of their surfaces.

ACKNOWLEDGMENT

The Al foils used in this paper were supplied from Toyo Aluminum K.K.

REFERENCES

- [1] H. Kamitsuna, "A very small, low-loss MMIC rat-race hybrid using elevated coplanar waveguides," *IEEE Microw. Guided Wave Lett.*, vol. 2, no. 8, pp. 337–339, Aug. 1992. doi: [10.1109/75.153606](https://doi.org/10.1109/75.153606).
- [2] H. Nakamura, T. Ishizaki, T. Nakatani, and S. Tsuzaki, "A new design concept for balanced-type SAW filters using a common-mode signal suppression circuit," *IEICE Trans. Electron.*, vol. E88-C, no. 1, pp. 28–33, 2005. doi: [10.1093/ietele/e88-c.1.28](https://doi.org/10.1093/ietele/e88-c.1.28).
- [3] H.-C. Jeong and K.-W. Yeom, "A design of X-band 40 W pulse-driven GaN HEMT power amplifier," *IEICE Trans. Electron.*, vol. E96-C, no. 6, pp. 923–934, 2013. doi: [10.1587/transele.E96.C.923](https://doi.org/10.1587/transele.E96.C.923).

- [4] T. Makita, I. Tamai, and S. Seki, "Coplanar waveguides on high-resistivity silicon substrates with attenuation constant lower than 1 dB/mm for microwave and millimeter-wave bands," *IEEE Trans. Electron Devices*, vol. 58, no. 3, pp. 709–715, Jan. 2011. doi: [10.1109/TED.2010.2098878](https://doi.org/10.1109/TED.2010.2098878).
- [5] E. Chen and S. Y. Chou, "Characteristics of coplanar transmission lines on multilayer substrates: Modeling and experiments," *IEEE Trans. Microw. Theory Techn.*, vol. 45, no. 6, pp. 939–945, Jun. 1997. doi: [10.1109/22.588606](https://doi.org/10.1109/22.588606).
- [6] J. Hu, A. Sligar, C.-H. Chang, S.-L. Lu, and R. K. Settaluri, "A grounded coplanar waveguide structure for microwave measurement of complex permittivity and permeability," *IEEE Trans. Magn.*, vol. 42, no. 7, pp. 1929–1931, Jul. 2006. doi: [10.1109/TMAG.2006.874098](https://doi.org/10.1109/TMAG.2006.874098).
- [7] L. Zhang *et al.*, "RF transmission properties of graphene with coplanar waveguide structure," *ECS Trans.*, vol. 60, no. 1, pp. 1087–1092, 2014. doi: [10.1149/06001.1087ecst](https://doi.org/10.1149/06001.1087ecst).
- [8] X. Wang, W. Chen, Z. Qin, D. Yang, M. Cai, and M. Yun, "The insertion loss of coplanar waveguide structure on PMNT thin films," in *Proc. IEEE Int. Conf. Microw. Millim. Wave Technol. (ICMMT)*, Beijing, China, Jun. 2016, pp. 473–475. doi: [10.1109/ICMMT.2016.7761812](https://doi.org/10.1109/ICMMT.2016.7761812).
- [9] Z. Wang, X. Shu, P. Peng, Y. Jia, and L. Ren, "Low insertion loss of 200 μm -long graphite coplanar waveguide," *Appl. Phys. Lett.*, vol. 108, no. 3, 2016, Art. no. 033104. doi: [10.1063/1.4940022](https://doi.org/10.1063/1.4940022).
- [10] K. C. Gupta, R. Garg, I. Bahl, and P. Bhartia, "Coplanar lines: Coplanar waveguide and coplanar strips," in *Microstrip Lines and Slotlines*, 2nd ed. Norwood, MA, USA: Artech House, 1996, pp. 375–456.
- [11] A. B. Menicanin, L. D. Zivanov, M. S. Damjanovic, and A. M. Maric, "Low-cost CPW meander inductors utilizing ink-jet printing on flexible substrate for high-frequency applications," *IEEE Trans. Electron Devices*, vol. 60, no. 2, pp. 827–832, Jan. 2013. doi: [10.1109/TED.2012.2234461](https://doi.org/10.1109/TED.2012.2234461).
- [12] J. N. Burghartz and B. Rejaei, "On the design of RF spiral inductors on silicon," *IEEE Trans. Electron Devices*, vol. 50, no. 3, pp. 718–729, Mar. 2003. doi: [10.1109/TED.2003.810474](https://doi.org/10.1109/TED.2003.810474).
- [13] V. N. R. Vanukuru, "High-Q inductors utilizing thick metals and dense-tapered spirals," *IEEE Trans. Electron Devices*, vol. 62, no. 9, pp. 3095–3099, Sep. 2015. doi: [10.1109/TED.2015.2458772](https://doi.org/10.1109/TED.2015.2458772).
- [14] J. Liang, T. Miyazaki, M. Morimoto, S. Nishida, N. Watanabe, and N. Shigekawa, "Electrical properties of p-Si/n-GaAs heterojunctions by using surface-activated bonding," *Appl. Phys. Express*, vol. 6, no. 2, 2013, Art. no. 021801. doi: [10.7567/APEX.6.021801](https://doi.org/10.7567/APEX.6.021801).
- [15] J. Liang, T. Miyazaki, M. Morimoto, S. Nishida, and N. Shigekawa, "Electrical properties of Si/Si interfaces by using surface-activated bonding," *J. Appl. Phys.*, vol. 114, Nov. 2013, Art. no. 183703. doi: [10.1063/1.4829676](https://doi.org/10.1063/1.4829676).
- [16] B. Rebhan, A. Hinterreiter, N. Malik, K. S.-Henriksen, V. Dragoi, and K. Hingerl, "Low-temperature aluminum-aluminum wafer bonding," *ECS Trans.*, vol. 75, no. 9, pp. 15–24, 2016. doi: [10.1149/07509.0015ecst](https://doi.org/10.1149/07509.0015ecst).
- [17] N. Shigekawa, J. Liang, R. Onitsuka, T. Agui, H. Juso, and T. Takamoto, "Current-voltage and spectral-response characteristics of surface-activated-bonding-based InGaP/GaAs/Si hybrid triple-junction cells," *Jpn. J. Appl. Phys.*, vol. 54, Jul. 2015, Art. no. 08KE03. doi: [10.7567/JJAP.54.08KE03](https://doi.org/10.7567/JJAP.54.08KE03).
- [18] J. Liang, K. Furuna, M. Matsubara, M. Dhamrin, Y. Nishio, and N. Shigekawa, "Aluminum foil/Si direct bonding as prototypes of ultrathick metal contacts in devices," *ECS J. Solid State Sci. Technol.*, vol. 6, no. 9, pp. 626–632, 2017. doi: [10.1149/2.0251709jss](https://doi.org/10.1149/2.0251709jss).
- [19] S. Morita, J. Liang, M. Matsubara, M. Dhamrin, Y. Nishio, and N. Shigekawa, "Electrical properties of Al foil/n-4H-SiC Schottky junctions fabricated by surface-activated bonding," *Jpn. J. Appl. Phys.*, vol. 57, Nov. 2018, Art. no. 02BE01. doi: [10.7567/JJAP.57.02BE01](https://doi.org/10.7567/JJAP.57.02BE01).
- [20] K. Matsuura, J. Liang, K. Maezawa, and N. Shigekawa, "Al-foil-based low-loss coplanar waveguides directly bonded to sapphire substrates," in *Proc. Int. Conf. Solid State Devices Mater. Extended Abstr.*, Sendai, Japan, 2017, pp. 495–496.
- [21] K. Okada and K. Masu, "Advanced microwave circuits and systems," in *Modeling of Spiral Inductors*. Rijeka, Croatia: InTech, 2010, pp. 291–312.
- [22] G. Stojanović, L. Živanov, and M. Damjanović, "Compact form of expressions for inductance calculation of meander inductors," *Serbian J. Elect. Eng.*, vol. 1, no. 3, pp. 57–68, 2004. doi: [10.2298/SJEE0403057S](https://doi.org/10.2298/SJEE0403057S).
- [23] T. H. Lee, "Characteristics of passive IC components," in *The Design of CMOS Radio-Frequency Integrated Circuits*, 2nd ed. Cambridge, U.K.: Cambridge Univ. Press, 2004, pp. 136–148.
- [24] C. Schollhorn, W. Zhao, M. Morschbach, and E. Kasper, "Attenuation mechanisms of aluminum millimeter-wave coplanar waveguides on silicon," *IEEE Trans. Electron Devices*, vol. 50, no. 3, pp. 740–746, Mar. 2003. doi: [10.1109/TED.2003.810466](https://doi.org/10.1109/TED.2003.810466).
- [25] J. Krupka, K. Derzakowski, M. Tobar, J. Hartnett, and R. G. Geyer, "Complex permittivity of some ultralow loss dielectric crystals at cryogenic temperatures," *Meas. Sci. Technol.*, vol. 10, no. 5, pp. 387–392, 1999. doi: [10.1088/0957-0233/10/5/308](https://doi.org/10.1088/0957-0233/10/5/308).